Time-dependent complete-active-space self-consistent-field method for multielectron dynamics in intense laser fields

Takeshi Sato[*] and Kenichi L. Ishikawa[†]

Photon Science Center, Graduate School of Engineering, The University of Tokyo, 7-3-1 Hongo, Bunkyo-ku, Tokyo 113-8656, Japan

The time-dependent complete-active-space self-consistent-field (TD-CASSCF) method for the description of multielectron dynamics in intense laser fields is presented, and a comprehensive description of the method is given. It introduces the concept of frozen-core (to model tightly bound electrons with no response to the field), dynamical-core (to model electrons tightly bound but responding to the field), and active (fully correlated to describe ionizing electrons) orbital subspaces, allowing compact yet accurate representation of ionization dynamics in many-electron systems. The classification into the subspaces can be done flexibly, according to simulated physical situations and desired accuracy, and the multiconfiguration time-dependent Hartree-Fock (MCTDHF) approach is included as a special case. To assess its performance, we apply the TD-CASSCF method to the ionization dynamics of one-dimensional lithium hydride (LiH) and LiH dimer models, and confirm that the present method closely reproduces rigorous MCTDHF results if active orbital space is chosen large enough to include appreciably ionizing electrons. The TD-CASSCF method will open a way to the first-principles theoretical study of intense-field-induced ultrafast phenomena in realistic atoms and molecules.

I. INTRODUCTION

The advent of the chirped pulse amplification (CPA) technique [1] has enabled the production of femtosecond laser pulses whose focused intensity easily exceeds 10^{14} W/cm^2 and even reaches $\sim 10^{22}$ W/cm^2 [2–4]. Exposed to visible-to-midinfrared pulses with an intensity typically higher than 10^{14} W/cm^2, atoms and molecules exhibit nonperturbative nonlinear response such as above-threshold ionization (ATI), tunneling ionization, high-order harmonic generation (HHG), and nonsequential double ionization (NSDI) [5,6]. HHG, for example, represents a highly successful avenue toward an ultrashort coherent light source in the extreme-ultraviolet (XUV) and soft x-ray regions [7,8]. The development of these novel light sources has opened new research possibilities including ultrafast molecular probing [9–11], attosecond science [12–14], and XUV nonlinear optics [15,16].

In parallel with the progress in experimental techniques, various numerical methods have been developed to explore atomic and molecular dynamics in intense laser fields. While direct solution of the time-dependent Schrödinger equation (TDSE) provides an exact description, this method is virtually unfeasible for multielectron systems beyond He [17–29] and H$_2$ [30–32]. As a result, the single-active electron (SAE) approximation is widely used, in which only the outermost electron is explicitly treated, and the effect of the others, assumed to be frozen, is embedded in a model potential. This approximation, however, fails to account for multielectron and multichannel effects [10,33–37] in high-field phenomena. Thus, alternative many-electron methods are required to catch up with new experimental possibilities. For example, Caillat *et al*. [38] have introduced the multiconfiguration time-

dependent Hartree-Fock (MCTDHF) approach (see below) to study correlated multielectron systems in strong laser fields. Although they have presented the results for up to six-electron model molecules, its computational time prohibitively increases with the number of electrons. Another interesting route is the time-dependent configuration-interaction singles (TD-CIS) method, implemented by Santra and co-workers [39,40], in which the many-electron wave function is expanded in terms of the Hartree-Fock (HF) ground state and singly excited configuration state functions (CSF). The TD-CIS method has an advantage to give a clear one-electron picture for multichannel ionizations. However, its applications are limited to the dynamics dominated by single ionizations, with an initial state described correctly by the HF method. Time-dependent density functional theory (TDDFT) [41–43], though attractive for its low computational cost, delivers only the electron density, not the wave function, rendering the definition of observables difficult. More seriously, it is difficult to estimate and systematically improve the accuracy of the exchange-correlation potential.

Among the more recent developments, the orbital-adapted time-dependent coupled-cluster (OATDCC) method proposed by Kvaal [44] is of particular interest, which pioneered the time-dependent coupled-cluster (CC) approach with bivariationally adapted orbital functions and excitation amplitudes. The fixed-orbital CC method was also implemented by Huber and Klamroth [45]. The time-dependent CC approach should be a promising avenue to the time-dependent many-electron problems in view of the spectacular success of the stationary CC theory. However, it seems to require further theoretical sophistications to make a rigorous numerical method of it. Hochstuhl and Bonitz proposed the time-dependent restricted-active-space configuration-interaction (RASCI) method [46], in which the total wave function is expanded with fixed Slater determinants compatible to the restricted-active-space constraints known in quantum chemistry [47]. The TD-RASCI

---
[*]sato@atto.t.u-tokyo.ac.jp
[†]ishiken@atto.t.u-tokyo.ac.jp

method, with cleverly devised spatial partitioning, has been successfully applied to helium and beryllium atoms [46]. A disadvantage of the method is the lack of the size extensivity [48,49] discussed in Sec. III, which is a common problem of truncated configuration-interaction (CI) approaches, except the simplest TD-CIS [39].

In this work, we propose a flexible *ab initio* time-dependent many-electron method based on the concept of the complete active-space self-consistent field (CASSCF) [50–53]. Our approach is derived from the first principles, and simultaneously, fills the huge gap between the MCTDHF method and SAE approximation.

Most of the ground-state closed-shell systems are described qualitatively well by the HF method [48]. However, the time-dependent Hartree-Fock (TDHF) method cannot describe ionization processes [54], since it is enforced to keep the initial closed-shell structure. Instead, at least two orbital functions are required to describe the field ionization of a singlet two-electron system. The spatial part of the total wave function in such approximations reads

$$\Psi(1,2) \propto \psi_1(1)\psi_2(2) + \psi_2(1)\psi_1(2) \tag{1a}$$

$$= C_1\phi_1(1)\phi_1(2) + C_2\phi_2(1)\phi_2(2). \tag{1b}$$

The first form is known as the extended Hartree-Fock (EHF) [55–57] wave function and has been successfully applied to the intense-field phenomena for two-electron systems [55,57,58]. The second form is obtained by the canonical orthogonalization of nonorthogonal orbitals $\psi_{i=1,2}$ [48], and is an example of the CI wave function [48,49]. It is clear that not only the CI coefficients $\{C_i(t)\}$ but also the orbitals $\{\phi_i(t)\}$ have to be varied in time in order to properly describe the ionization. Thus we need the multiconfiguration Hartree-Fock (MCHF) or the multiconfiguration self-consistent-field (MC-SCF) wave function [48,49,53], where both the CI coefficients and the shape of the orbitals are the variational degrees of freedom.

This idea has been realized for many-electron systems by the MCTDHF method [38,59], in which the total wave function is expanded in terms of Slater determinant (or CSF) bases,

$$\Psi(t) = \sum_I C_I(t)\Phi_I(t), \tag{2}$$

where both CI coefficients $\{C_I(t)\}$ and bases $\{\Phi_I(t)\}$ are allowed to vary in time. The Slater determinants are constructed (in the spin-restricted treatment, see Sec. II A) from $2n$ spin orbitals $\{\phi_p; p = 1, 2, \ldots n\} \otimes \{\alpha, \beta\}$, where $\{\phi_p(t)\}$ are time-dependent spatial orbital functions and α (β) is the up- (down-) spin eigenfunction. See also Refs. [60–66] for the MCTDHF method, and Beck *et al.* [67] and references therein for the precedent multiconfiguration time-dependent Hartree method for Bosons.

Despite its naming, which in principle refers to the *general* multiconfiguration wave function of the form Eq. (2) with flexible choice of expansion bases (range of summation I), previous implementations of the MCTDHF method (except the fixed-CI formulation of Ref. [66]) were limited to the full-CI expansion; the summation I of Eq. (2) is over all the possible ways of distributing N electrons among the $2n$ spin

orbitals. More intuitively, we write such an MCTDHF wave function symbolically as

$$\Psi_{\text{MCTDHF}} : \{\phi_1(t)\phi_2(t)\ldots\phi_n(t)\}^N, \tag{3}$$

which is understood to represent the N-electron full-CI wave function using n time-dependent orbitals. Though powerful, the MCTDHF method suffers from severe limitation in the applicability to large systems, since the full-CI dimension grows factorially with increasing N.

It is reasonable to expect that in a large molecule interacting with high-intensity, long-wavelength lasers, the deeply bound electrons remain nonionized, while only the higher-lying valence electrons ionize appreciably. For the bound electrons, a closed-shell description of the HF type would be acceptable as a first approximation [68]. On the other hand, correlated treatment is required for ionizing electrons to describe the seamless transition from the closed-shell-dominant initial state into the symmetry-breaking continuum (discussed in Sec. III B).

The CASSCF method [50–53] provides an ideal *ansatz* for such a problem. It introduces the concept of *core* and *active* orbital subspaces, and spatial orbitals participating in Eq. (3) are classified into these subspaces. The core orbitals are forced to be doubly occupied all the time, while the active orbitals are allowed general (0, 1, or 2) occupancies. Thus, the CASSCF wave function is written symbolically as

$$\Psi_{\text{CASSCF}}(t) : \phi_1^2\phi_2^2 \cdots \phi_{n_C}^2 \tag{4a}$$

$$\times \left\{\phi_{n_C+1}\phi_{n_C+2} \cdots \phi_{n_C+n_A}\right\}^{N_A}, \tag{4b}$$

where factors (4a) and (4b) represent core and active subspaces, respectively, and the total wave function is properly antisymmetrized. See Sec. II A for the rigorous definition. The n_C *core orbitals* describe $N_C = n_C/2$ *core electrons* within the closed-shell constraint, while the N_A *active electrons* are fully correlated using n_A *active orbitals*. Whereas, in general, all the orbitals are varied in time, it is also possible to further split the core space into *frozen-core* (fixed) and *dynamical-core* (allowed to vary in time in response to the field) subspaces. See Fig. 1, which illustrates the concept of the orbital subspacing.

The equation of motion (EOM) of our method, called TD-CASSCF, is derived based on the time-dependent variational principle (TDVP) [69–71], as detailed in Sec. II. It guarantees the best possible solution using the total wave function expressed as Eq. (4). The fully correlated active space enables a correct description of ionization processes which involve the strong correlation caused by the breaking closed-shell symmetry (discussed in Sec. III B). It can also include multichannel and multielectron effects (discussed in Sec. III C). The dynamical core orbitals account for the effect of field-induced core polarizations. In whole, the TD-CASSCF method enables compact yet accurate representation of multielectron dynamics, if the active space is chosen correctly according to the physical processes of interest.

This paper proceeds as follows. In Sec. II, the details of the TD-CASSCF method are described. Then in Sec. III, the TD-CASSCF method is numerically assessed for ionization dynamics of one-dimensional multielectron models. Finally, Sec. IV concludes this work and discusses future prospects.
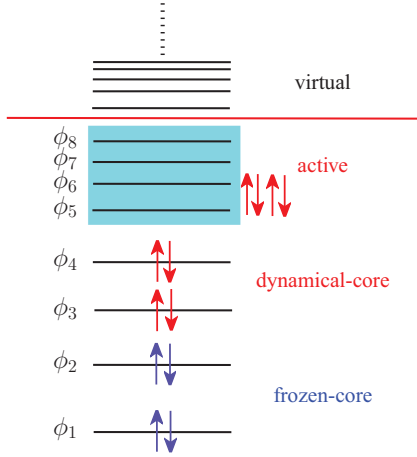
FIG. 1. (Color online) Pictorial explanation of the TD-CASSCF concept, illustrating a 12-electron system with two frozen-core (orbitals 1 and 2), two dynamical-core (3 and 4), and four active orbitals (5 to 8). Solving the orbital-EOM guarantees the variational splitting, in a time-dependent sense, of core-active, core-virtual, and active-virtual orbital subspaces.

Appendix provides the definition and computational details for real-space domain-based ionization probabilities. The Hartree atomic units are used throughout unless otherwise noted.

II. THEORY

In this section, we derive the EOMs for the TD-CASSCF method. To this end, first we give the rigorous definitions of the MCTDHF, MCSCF, CASSCF, and general multiconfiguration *ansatz* for the total wave function in Sec. II A. Next in Sec. II B, the EOMs of orbitals and CI coefficients for the general multiconfiguration wave functions are discussed by reviewing the work of Miranda *et al.* [66]. Then we specialize the general formulation to the TD-CASSCF method in Sec. II C to derive the explicit EOMs, and discuss its computational aspects in Sec. II D.

A. Multiconfiguration wave functions

Our formulation is determinant-based [47,65,72] within the spin-restricted treatment, i.e., using the same spatial orbitals for up- and down-spin electrons. We define *n occupied* spatial orbitals $\{\phi_p; p = 1,2,\ldots,n\}$ and $N_b - n$ *virtual* orbitals $\{\phi_a; a = n + 1, n + 2, \ldots, N_b\}$, where N_b is the dimension of the spinless one-particle Hilbert space, determined by, e.g., the number of grid points to discretize the orbitals or the number of intrinsic single-particle basis functions to expand the orbitals. The indices $\{p,q,r,s\}$, $\{a,b\}$, and $\{\mu,\nu,\lambda,\gamma,\delta\}$ are used to label occupied, virtual, and general (occupied + virtual) orbitals, respectively, and $\{\sigma,\tau\} \in \{\alpha,\beta\}$ label spin eigenfunctions. In the following, Einstein's summation convention is applied for repeated orbital indices within a term, with summation ranges implicit as above. The orbitals are assumed to be orthonormal all the time,

$$\langle\phi_\mu(t)|\phi_\nu(t)\rangle \equiv \int d\mathbf{r}\,\phi_\mu^*(t)\phi_\nu(t) = \delta_\nu^\mu, \qquad (5)$$

where δ_ν^μ denotes the Kronecker delta. The Slater determinants $\Phi_I(t)$ in Eq. (2) are constructed from the occupied orbitals $\{\phi_p\}$, and given in the occupation number representation [49,65] as

$$|I(t)\rangle = \left|I_1^\alpha I_2^\alpha \cdots I_n^\alpha I_1^\beta I_2^\beta \cdots I_n^\beta; t\right\rangle$$
$$= \prod_{p=1}^n (\hat{a}_{p\alpha}^\dagger)^{I_p^\alpha}(\hat{a}_{p\beta}^\dagger)^{I_p^\beta}|vac\rangle, \qquad (6)$$

where $\hat{a}_{\mu\sigma}^\dagger$ (and $\hat{a}_{\mu\sigma}$ appearing below) is the fermion creation (destruction) operator for $2N_b$ spin orbitals $\{\phi_\mu\} \otimes \{\alpha,\beta\}$. The integer array $\{I_p^\sigma = 0,1\}$ specifies the occupancy of each spin orbital, where $\sum_{p=1}^n I_p^\sigma = N^\sigma$, with N^σ being the number of σ-spin electrons, and $N = N^\alpha + N^\beta$. The time dependence of the occupation number vector $|I(t)\rangle$ is implicit in the spatial orbitals.

We focus on the dynamics induced by spin-independent external fields, and the initial wave function is assumed to be the spin eigenfunction. Therefore the total and projected spin operators $(\hat{S}^2,\hat{S}_z)$ are the constants of motion. Each Slater determinant is the eigenfunction of $\hat{S}_z$ with eigenvalue $(N^\alpha - N^\beta)/2$, while not generally of $\hat{S}^2$. However, the variational optimization of an initial state normally gives proper spin combinations, especially for the singlet ground state. See, e.g., Ref. [72], for a working protocol to obtain the spin-adapted solutions, within the determinant-based approach, for more complex electronic structures.

Throughout this paper, the term MCTDHF is used for the method based on the full-CI expansion using n occupied orbitals:

$$|\Psi_{\mathrm{MCTDHF}}(t)\rangle = \sum_I^{\Pi_{\mathrm{FCI}}} C_I(t)|I(t)\rangle, \qquad (7)$$

with I varying freely in the full-CI space Π_{FCI}, spanned by all the determinants generated from the $2n$ occupied spin orbitals. This is the current standard of the MCTDHF method as mentioned in Sec. I. Note that Miranda *et al.* [66] used the term MCTDHF in a broader sense to denote approaches based on the *general* multiconfiguration wave functions. To be definite, we call the general *ansatz* as MCSCF:

$$|\Psi_{\mathrm{MCSCF}}(t)\rangle = \sum_I^{\Pi} C_I(t)|I(t)\rangle, \qquad (8)$$

with the general CI space Π defined as any arbitrary subspace of Π_{FCI}, $\Pi = \{|I\rangle \in \Pi_{\mathrm{FCI}}; C_I(t) \not\equiv 0\}$. A trivial example of this class is the single-determinant HF wave function for closed-shell singlet or open-shell high-spin states. The only nontrivial applications of Eq. (8) to the time-dependent problems made thus far is the general open-shell TDHF approaches formulated in Ref. [66], in which the CI coefficients are determined by the spin symmetry and are time independent.

One of the most important MCSCF methods in quantum chemistry is the CASSCF (also known as fully optimized reaction space) method introduced in Sec. I [Eq. (4)], in which the CI expansion is limited to the space spanned by Slater determinants that include n_C doubly occupied core orbitals,

called the CASCI space Π_{CAS}:

$$|\Psi_{CASSCF}(t)\rangle = \sum_I^{\Pi_{CAS}} C_I(t)|I(t)\rangle, \tag{9}$$

$$|I\rangle = \prod_{i=1}^{n_C} \hat{a}_{i\alpha}^\dagger \hat{a}_{i\beta}^\dagger \prod_{t=n_C+1}^{n} (\hat{a}_{t\alpha}^\dagger)^{I_t^\alpha} (\hat{a}_{t\beta}^\dagger)^{I_t^\beta} |vac\rangle, \tag{10}$$

with $\sum_t I_t^\sigma = N_A^\sigma$ being the number of σ-spin active electrons satisfying $N_A^\sigma = N^\sigma - N_C/2$ and $N_A = N_A^\alpha + N_A^\beta$. Hereafter, we use orbital indices $\{i,j,k,l\}$ for core orbitals and $\{t,u,v,w,x\}$ for active orbitals, while keeping $\{p,q,r,s\}$ for general occupied (core + active) orbitals. Following the convention in the electronic structure theory [48,49], we use the acronym CASSCF(N_A,n_A) to denote the CASSCF wave function with N_A active electrons and n_A active orbitals. The MCTDHF wave function with n occupied orbitals is identical to CASSCF(N,n) and denoted as MCTDHF(n). See Fig. 1, Eqs. (3) and (4) in Sec. I, and Eqs. (50) and (51) in Sec. III, for intuitive understanding of these notations.

B. Equations of motion for MCSCF wave functions

Recently, Miranda *et al.* discussed EOMs for MCSCF wave functions [66]. Although their main motivation was the fixed-CI formulations, they also presented important equations applicable to the general MCSCF wave functions (see Sec. IV of Ref. [66]). Here we follow the essentials of their development to obtain Eqs. (20) and (21) below.

The spin-free second-quantized Hamiltonian is given by

$$\hat{H} = h_\nu^\mu \hat{E}_\nu^\mu + \frac{1}{2} g_{\nu\gamma}^{\mu\lambda} \hat{E}_{\nu\gamma}^{\mu\lambda}, \tag{11}$$

where h_ν^μ and $g_{\nu\gamma}^{\mu\lambda}$ are the one- and two-electron Hamiltonian matrix elements,

$$h_\nu^\mu = \int d\boldsymbol{r} \phi_\mu^*(\boldsymbol{r}) h(\boldsymbol{r},\nabla_r) \phi_\nu(\boldsymbol{r}), \tag{12}$$

$$g_{\nu\gamma}^{\mu\lambda} = \iint d\boldsymbol{r}_1 d\boldsymbol{r}_2 \phi_\mu^*(\boldsymbol{r}_1)\phi_\lambda^*(\boldsymbol{r}_2) V_{ee}(\boldsymbol{r}_1,\boldsymbol{r}_2) \times \phi_\nu(\boldsymbol{r}_1)\phi_\gamma(\boldsymbol{r}_2), \tag{13}$$

with h consisting of kinetic, nucleus-electron, and external laser terms, and V_{ee} being the electron-electron interaction, and

$$\hat{E}_\nu^\mu = \sum_\sigma \hat{a}_{\mu\sigma}^\dagger \hat{a}_{\nu\sigma}, \tag{14}$$

$$\hat{E}_{\nu\gamma}^{\mu\lambda} = \sum_{\sigma\tau} \hat{a}_{\mu\sigma}^\dagger \hat{a}_{\lambda\tau}^\dagger \hat{a}_{\gamma\tau} \hat{a}_{\nu\sigma} = \hat{E}_\nu^\mu \hat{E}_\gamma^\lambda - \hat{E}_\gamma^\mu \delta_\nu^\lambda. \tag{15}$$

Following the TDVP [69–71], the action integral S,

$$S[\Psi] = \int_{t_0}^{t_1} dt \langle \Psi | \left(\hat{H} - i\frac{\partial}{\partial t} \right) |\Psi\rangle, \tag{16}$$

is made stationary,

$$\delta S = \int_{t_0}^{t_1} dt \{ \langle \delta\Psi | (\hat{H}|\Psi\rangle - i|\dot{\Psi}\rangle) + (\langle\Psi|\hat{H} + i\langle\dot{\Psi}|)|\delta\Psi\rangle \} = 0, \tag{17}$$

with respect to allowed variations $\delta\Psi$ of the total wave function, where $\dot{\Psi} \equiv \partial\Psi/\partial t$. The time derivative of $\delta\Psi$ is integrated out by part, assuming $\delta\Psi(t_0) = \delta\Psi(t_1) = 0$. See Ref. [71] for the formal discussion on the validity of this

procedure. By taking the orbital orthonormality into account, the variations and the time derivatives of an orbital ϕ_μ can be written as $\delta\phi_\mu = \phi_\nu \Delta_\mu^\nu$ and $i\dot{\phi}_\mu = \phi_\nu R_\mu^\nu$, respectively, with $R_\nu^\mu \equiv i\langle\phi_\mu|\dot{\phi}_\nu\rangle$. The matrix Δ is anti-Hermitian, while R is Hermitian [66]. Then the allowed variation and the time derivative of the total wave function are compactly given by

$$|\delta\Psi\rangle = \sum_I^\Pi |I\rangle \delta C_I + \hat{\Delta}|\Psi\rangle, \tag{18}$$

$$i|\dot{\Psi}\rangle = i\sum_I^\Pi |I\rangle \dot{C}_I + \hat{R}|\Psi\rangle, \tag{19}$$

where δC_I and $\dot{C}_I$ are the variation and the time derivative of the CI coefficient C_I, and $\hat{\Delta} = \Delta_\nu^\mu \hat{E}_\nu^\mu$, $\hat{R} = R_\nu^\mu \hat{E}_\nu^\mu$. Inserting Eqs. (18) and (19) and their Hermitian conjugates $\langle\delta\Phi|$ and $-i\langle\dot{\Phi}|$ into Eq. (17), and requiring the equality for individual variations $\delta C_I(t)$ and $\Delta_\nu^\mu(t)$, after some algebraic manipulations [66] we have

$$i\dot{C}_I = \langle I|\bar{H}|\Psi\rangle, \tag{20}$$

$$\langle\Psi|\bar{H}(1-\hat{\Pi})\hat{E}_\nu^\mu|\Psi\rangle - \langle\Psi|\hat{E}_\nu^\mu(1-\hat{\Pi})\bar{H}|\Psi\rangle = 0, \tag{21}$$

where $\bar{H} = \hat{H} - \hat{R}$, and $\hat{\Pi} = \sum_{I\in\Pi} |I\rangle\langle I|$ is the configuration projector onto the general CI space Π. The system of equations, Eqs. (20) and (21), is to be solved for $i\dot{C}_I$ and R, which determine the time dependence of CI coefficients and orbitals, respectively. In Ref. [66], these equations appeared as an intermediate to derive the MCTDHF equation, rather than as the final result. Here we emphasize that Eqs. (20) and (21) are valid for *general* MCSCF wave function fit into the form of Eq. (8). Equation (21) is also extensively discussed by Miyagi and Madsen in their recent development of the MCTDHF method with restricted CI expansions [73].

C. TD-CASSCF equations of motion

1. Orbital equations of motion

Now we apply the CASSCF constraint defined in Sec. II A to the general orbital-EOM derived in Sec. II B. Equation (21), with $\hat{\Pi}$ replaced by $\hat{\Pi}_{CAS}$, reduces to a trivial identity for an orbital pair $\{\mu,\nu\}$ belonging to a same orbital subspace (core, active, or virtual), since the singly replaced determinants, $\hat{E}_j^i|I\rangle = 2\delta_j^i|I\rangle$, $\hat{E}_u^t|I\rangle$, or $\hat{E}_b^a|I\rangle = 0$, either fall within Π_{CAS} or vanish, and the configuration projector $1 - \hat{\Pi}_{CAS}$ eliminates such contributions. We refer to these intrasubspace orbital rotations $\hat{E}_\nu^\mu = \{\hat{E}_j^i, \hat{E}_u^t, \hat{E}_b^a\}$ as *redundant*, since the total wave function is invariant under such orbital transformations, if accompanied by the corresponding transformation of CI coefficients [38,49]. For the redundant orbital pairs, one can freely choose R_ν^μ to be the matrix element

$$R_\nu^\mu = \langle\phi_\mu|\hat{\theta}(t)|\phi_\nu\rangle \tag{22}$$

of an arbitrary one-electron Hermitian operator $\hat{\theta}(t)$ [38].

Next, for orbital pairs $\{\mu,\nu\}$ belonging to different subspaces (core-active, core-virtual, or active-virtual), the projector $\hat{\Pi}_{CAS}$ can be dropped in Eq. (21), since $\hat{E}_\nu^\mu|\Psi\rangle$ is not included in Π_{CAS}, and we have a simpler expression,

$$\langle\Psi|[\hat{H} - \hat{R}, \hat{E}_\nu^\mu]|\Psi\rangle = 0, \tag{23}$$

with $\hat{E}_\nu^\mu = \{\hat{E}_p^a, \hat{E}_a^p, \hat{E}_i^t, \hat{E}_t^i\}$ constituting the *nonredundant* orbital rotations. The general orbital-EOM of Eq. (21) is thus reduced to Eq. (23), which is to be solved only for the nonredundant orbital pairs.

It is fascinating to see an analogy in Eq. (23) with the time-independent MCSCF theory; it is formally identical to the generalized Brillouin condition of the stationary wave function [74,75], if we replace $\hat{H} - \hat{R}$ with $\hat{H}$. Thus the remaining derivations are parallel to the time-independent theory. We can explicitly write down the matrix elements of Eq. (23) to obtain

$$R_\lambda^\mu D_\nu^\lambda - D_\lambda^\mu R_\nu^\lambda = F_\nu^\mu - F_\mu^{\nu*}, \tag{24}$$

$$F_\nu^\mu = h_\lambda^\mu D_\nu^\lambda + g_{\lambda\delta}^{\mu\gamma} P_{\nu\gamma}^{\lambda\delta}, \tag{25}$$

where $D_\nu^\mu \equiv \langle\Psi|\hat{E}_\mu^\nu|\Psi\rangle$ and $P_{\nu\gamma}^{\mu\lambda} \equiv \langle\Psi|\hat{E}_{\mu\lambda}^{\nu\gamma}|\Psi\rangle$ are one- and two-electron reduced density matrix (RDM) elements, respectively. The matrix F is called the generalized Fock matrix, whose Hermiticity, leading to the vanishing right-hand side of Eq. (24), is the stationary condition with respect to the orbital variations [49,51–53].

The nonzero density matrix elements of the CASSCF wave function are $D_j^i = 2\delta_j^i, D_u^t, P_{kl}^{ij} = 4\delta_k^i\delta_l^j - 2\delta_l^i\delta_k^j, P_{ui}^{ti} = 2D_u^t, P_{iu}^{ti} = -D_u^t$, and P_{vw}^{tu}. Then the required generalized Fock matrix elements read [51]

$$F_i^\mu = 2\left(f_i^\mu + G_i^\mu\right), \tag{26}$$

$$F_t^\mu = f_u^\mu D_t^u + (\Gamma_t)_t^\mu, \tag{27}$$

where the matrices f, G, and Γ_t represent, respectively, operators $\hat{f}$, $\hat{G}$, and $\hat{\Gamma}_t$ given by

$$\hat{f} = \hat{h}^{\mathrm{FC}} + \sum_j^{\mathrm{d.c.}}(2\hat{J}_j - \hat{K}_j), \tag{28}$$

$$\hat{G} = \left(\hat{J}_u^t - \frac{1}{2}\hat{K}_u^t\right) D_t^u, \tag{29}$$

$$\hat{\Gamma}_t|\phi_t\rangle = \hat{W}_w^u|\phi_v\rangle P_{tu}^{vw}, \tag{30}$$

$$\hat{h}^{\mathrm{FC}}(t) = \hat{h}(t) + \sum_j^{\mathrm{f.c.}}\left(2\hat{J}_j(0) - \hat{K}_j(0)\right), \tag{31}$$

where summation j in Eqs. (28) and (31) are restricted within dynamical-core (d.c.) and frozen-core (f.c.) subspaces, respectively. The operators $\hat{f}$ and $\hat{G}$ are universal and Hermitian, while $\hat{\Gamma}_t$ is defined with an active orbital ϕ_t to be applied from the left and is non-Hermitian. We define Coulomb $\hat{J}$, exchange $\hat{K}$, and general $\hat{W}$ mean-field operators as $\hat{J}_p = \hat{J}_p^p, \hat{K}_p = \hat{K}_p^p, \hat{J}_q^p = \hat{W}_q^p, \hat{K}_q^p|\phi_r\rangle = \hat{W}_r^p|\phi_q\rangle)$, where $\hat{W}_q^p$ is local [63] and given in the coordinate space as

$$W_q^p(\boldsymbol{r}) = \int d\bar{\boldsymbol{r}} \phi_p^*(\bar{\boldsymbol{r}}) V_{ee}(\boldsymbol{r},\bar{\boldsymbol{r}}) \phi_q(\bar{\boldsymbol{r}}). \tag{32}$$

In Eq. (31), time argument t is explicitly attached to emphasize that the time dependence of the frozen-core dressed one-electron Hamiltonian $\hat{h}^{\mathrm{FC}}(t)$ comes entirely from the external laser field contribution in $\hat{h}(t)$. Now Eq. (24) for the time derivative matrix $R_\nu^\mu = \mathrm{i}\langle\phi_\mu|\dot{\phi}_\nu\rangle$ can be worked out for

intersubspace (nonredundant) elements:

$$R_i^\mu = R_\mu^{i*} = 0 \quad (i \in \mathrm{f.c.}), \tag{33}$$

$$R_i^a = R_a^{i*} = f_i^a + G_i^a \quad (i \in \mathrm{d.c.}), \tag{34}$$

$$R_t^a = R_a^{t*} = f_t^a + (\Gamma_u)_u^a (D^{-1})_t^u, \tag{35}$$

$$R_i^t = R_i^{i*} = f_i^t + (\bar{D}^{-1})_u^t \left\{G_i^u - (\Gamma_u)_i^u\right\} \tag{36}$$
$$(i \in \mathrm{d.c.}),$$

with $\bar{D}_u^t = 2\delta_u^t - D_u^t$.

One could, in principle, directly work with Eqs. (33)–(36) in the matrix formulation [59], which determines the time dependence of occupied $\{\phi_p(t)\}$, as well as virtual $\{\phi_a(t)\}$ orbitals. However, it is beneficial to introduce the orbital projector

$$\hat{Q} = \sum_a |\phi_a\rangle\langle\phi_a| = 1 - \sum_p |\phi_p\rangle\langle\phi_p| \tag{37}$$

onto the virtual orbital space to avoid (using the assumed completeness) explicitly dealing with numerous virtual orbitals [38,67]. Thus we arrive at the final expression of EOMs for dynamical-core and active orbitals as follows:

$$\mathrm{i}|\dot{\phi}_i\rangle = \hat{Q}(\hat{f} + \hat{G})|\phi_i\rangle + |\phi_p\rangle R_i^p, \tag{38}$$

$$\mathrm{i}|\dot{\phi}_t\rangle = \hat{Q}\left\{\hat{f}|\phi_t\rangle + \hat{\Gamma}_u|\phi_u\rangle(D^{-1})_t^u\right\} + |\phi_p\rangle R_t^p, \tag{39}$$

with R determined by Eqs. (36) for nonredundant pairs, and taken from Eq. (22) for redundant elements. The dynamics of the total wave function is independent of $\hat{\theta}$ in Eq. (22), but the choice of $\hat{\theta}$ affects the numerical stability and efficiency of the propagation scheme [38]. Solving Eqs. (36)–(39) guarantees the optimal separation, in the TDVP sense, of frozen-core, dynamical-core, active, and virtual orbital subspaces, as illustrated in Fig. 1. This ensures the gauge invariance of the TD-CASSCF method, since the orbital subspaces are stable against single excitations [Eq. (23)] arising with the transformation, e.g., from the length gauge to the velocity gauge.

2. CI equations of motion

The general CI-EOM of Eq. (20) is specialized to the TD-CASSCF method as

$$\mathrm{i}\dot{C}_I = \sum_J^{\Pi_{\mathrm{CAS}}} \left(H_{IJ}^{\mathrm{A}} - \delta_{IJ}E^{\mathrm{A}} - R_{IJ}\right) C_J, \tag{40}$$

where $R_{IJ} = \langle I|\hat{R}|J\rangle = \langle I|\hat{\theta}|J\rangle$, E^{A} and H_{IJ}^{A} are active orbital contributions to the total energy and determinant basis Hamiltonian matrix elements, respectively,

$$E \equiv \langle\Psi|\hat{H}|\Psi\rangle = E^{\mathrm{C}} + E^{\mathrm{A}}, \tag{41}$$

$$\langle I|\hat{H}|J\rangle = \delta_{IJ}E^{\mathrm{C}} + H_{IJ}^{\mathrm{A}}, \tag{42}$$

where

$$E^{\mathrm{C}} = \sum_i^{\mathrm{d.c.}} \left\{(h^{\mathrm{FC}})_i^i + f_i^i\right\}, \tag{43}$$

$$E^{\mathrm{A}} = f_u^t D_t^u + \tfrac{1}{2} g_{uw}^{tv} P_{tv}^{uw}, \tag{44}$$

$$H_{IJ}^{\mathrm{A}} = f_u^t (D_{IJ})_t^u + \tfrac{1}{2} g_{uw}^{tv} (P_{IJ})_{tv}^{uw}, \tag{45}$$

where $(D_{IJ})_t^u = \langle I|\hat{E}_u^t|J\rangle$ and $(P_{IJ})_{tv}^{uw} = \langle I|\hat{E}_{uw}^{tv}|J\rangle$. In Eq. (40), we make a particular phase choice, $\mathrm{i}\langle\Psi|\dot{\Psi}\rangle = 0$, by extracting the dynamical phase $\exp[-\mathrm{i}\int^t dt' E(t')]$ from the total wave function. This stabilizes the CI-EOM, especially when we have a large active space.

D. Computational remarks

The TD-CASSCF method includes as special cases both TDHF and MCTDHF methods, thus bridging the gap between the uncorrelated and fully correlated descriptions in a flexible way. A practical advantage of this generality is that a computational code written for the TD-CASSCF method can be used also for TDHF and MCTDHF calculations, by setting $\{n_C = n,\ n_A = 0\}$ and $\{n_C = 0,\ n_A = n\}$, respectively. It can also execute open-shell TDHF calculation with fixed CI coefficients [66]. One indeed finds close similarity between TD-CASSCF EOMs Eqs. (38)–(40) and those of the MCTDHF method (see, e.g., Ref. [65]). Naively, ingredients of the TD-CASSCF EOMs are the compilation of those for the TDHF (core orbitals) and MCTDHF (active orbitals and CI coefficients) methods. This means that an existing code for the MCTDHF method can be easily generalized to the TD-CASSCF method.

The computationally most demanding procedures required to integrate the TD-CASSCF EOMs are grouped into two categories:

(A) Calculations of 2RDM elements P_{vw}^{tu}, and the two-electron contributions of Eq. (40),

$$\mathrm{i}\dot{C}_I \longleftarrow \frac{1}{2}\sum_J^{\Pi_{\mathrm{CAS}}} g_{uw}^{tv}(P_{IJ})_{tv}^{uw} C_J. \tag{46}$$

The amount of work in these procedures roughly scales as $O[N_A^2(n_A - N_A)^2 N_{\mathrm{det}}]$ if $N_A^\alpha = N_A^\beta$ (see Ref. [47] for more details), where N_{det} is the number of determinants in Π_{CAS}, which in turn scales factorially with the number of active electrons N_A.

(B) Calculations of the mean fields $W_q^p(\mathbf{r})$, two-electron integrals g_{uw}^{tv}, and the 2RDM contributions in Eq. (39):

$$\mathrm{i}|\dot{\phi}_t\rangle \longleftarrow \hat{W}_w^v|\phi_x\rangle P_{uv}^{xw}(D^{-1})_t^u. \tag{47}$$

The computational cost of these steps depend explicitly on the number of grid points (or basis functions) N_b, as $O(n^2 N_b^2)$ for the mean fields and $O(n_A^4 N_b)$ for the others.

Important cost reductions are achieved for both procedures (A) and (B) by the TD-CASSCF method adopting core orbitals, compared to the MCTDHF method with the same number of occupied orbitals. The speedup and resource savings for procedure (A) are substantial due to the decreased CI dimension. This is especially the case if $N_A \ll N$, which is expected for an electronic structure with a few weakly bound valence and large numbers of physically inactive core electrons. The cost reduction for procedure (B) is not as drastic as for (A), since the amount of arithmetics $O(n^2 N_b^2)$ of computing mean fields $W_q^p(\mathbf{r})$ is independent of the CAS structure (only related to n). The computations of two electron integrals and Eq. (47) become much faster through restricting the orbital indices within the active instead of all occupied orbitals. The relative importance of these bottlenecks largely depends on

the problem at hand, and on the spatial representation of the orbitals and electron-electron interactions. This point will be discussed in Sec. III C.

III. NUMERICAL RESULTS AND DISCUSSIONS

In this section we apply the TD-CASSCF method to the ionization dynamics of one-dimensional (1D) multielectron model molecules. The effective 1D Hamiltonian for N electrons in the potential of M fixed nuclei interacting with an external laser electric field $E(t)$ is taken as

$$H = \sum_i^N \left\{ -\frac{1}{2}\frac{\partial^2}{\partial x_i^2} - \sum_a^M \frac{Z_a}{\sqrt{(x_i - X_a)^2 + c}} - E(t)x_i \right\}$$
$$+ \sum_{i>j}^N \frac{1}{\sqrt{(x_i - x_j)^2 + d}}, \tag{48}$$

where $x_i\ (i = 1, \ldots, N)$ is the position of the ith electron, $\mathbf{X} = \{X_a\}$ and $\mathbf{Z} = \{Z_a\}\ (a = 1, \ldots, M)$ are the positions and charges of nuclei, and c and d adjust the soft Coulomb operators of electron-nuclear and electron-electron interactions, respectively. The electron-laser interaction is included within the dipole approximation and in the length gauge. Note that the TD-CASSCF method is gauge-invariant, as mentioned in Sec. II C 1. We have performed some of the calculations described below also in the velocity gauge and confirmed that the results are virtually identical to those in the length gauge.

In this work, we make the simplest choice of $\hat{\theta}(t) \equiv 0$ [38] in Eq. (22), and therefore $R_{IJ} = 0$ in Eq. (40). The orbital-EOMs are discretized on an equidistant grid of spacing $\Delta x = 0.4$ (finer grid with $\Delta x = 0.1$ is used for drawing Figs. 2–4) within a simulation box $|x| < L = 600$. An absorbing boundary is implemented by the mask function of $\cos^{1/4}$ shape at
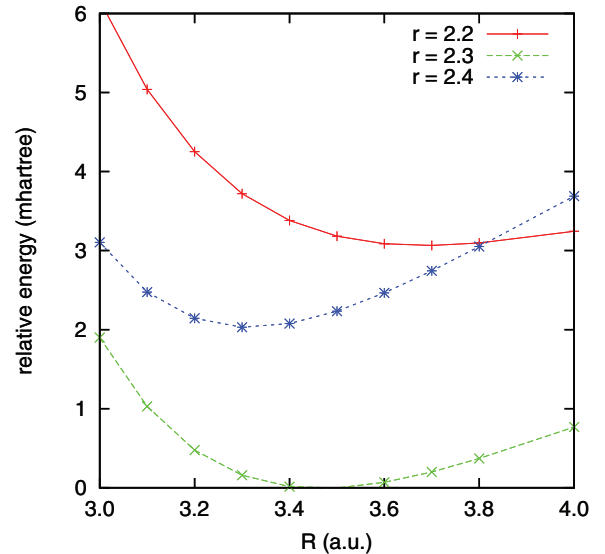

FIG. 2. (Color online) Several cuts of the adiabatic energy surface $E(r,R)$ of the 1D-$(\mathrm{LiH})_2$ model obtained by the MCTDHF(8) method. The energy of Eq. (49) is plotted [relative to the lowest energy of $E(r = 2.3, R = 3.5) = -14.182$ a.u.] against intermolecular LiH–LiH distance R for several bond lengths r of Li-H, constrained to be the same for two LiH molecules.
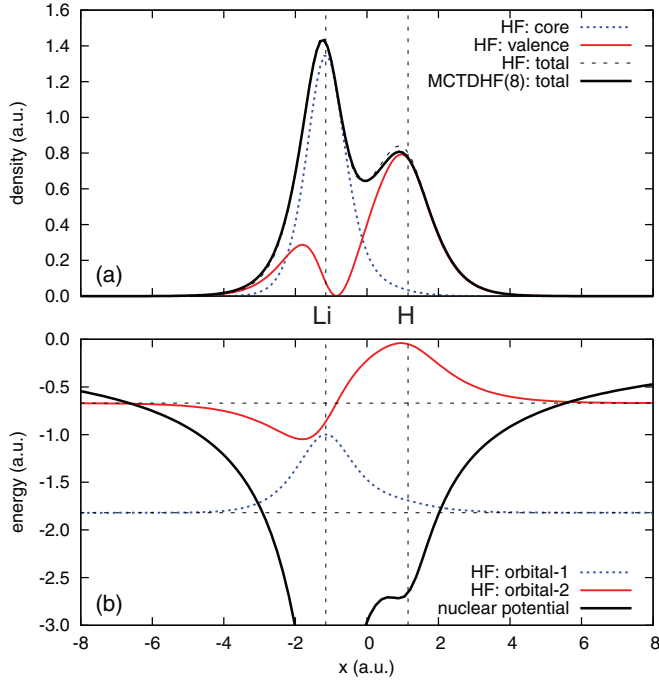
FIG. 3. (Color online) The ground-state electron density and occupied HF orbitals of the 1D-LiH model. (a) The total electron density by HF (black dashed) and MCTDHF(8) (black thick solid) methods are compared. The two lines closely overlap each other. Also shown are the core (orbital 1) and valence (orbital 2) contributions to the total HF density. (b) The occupied HF orbitals are drawn in an arbitrary scale vertically shifted by orbital energies -1.82 (orbital 1) and -0.67 (orbital 2). The solid curve and dashed vertical lines show the nuclear potential and positions of nuclei, respectively.

15% side edges of the box. The ground-state electronic structure is obtained by the imaginary time propagation with the fourth-order Runge-Kutta (RK4) algorithm with Schmidt orthonormalization of orbitals after each propagation [59]. The real-time propagations use a variable step-size embedded fourth- and fifth-order Runge-Kutta (VRK5) method. The kinetic energy operator $-\frac{1}{2}\frac{\partial^2}{\partial x_i^2}$ is evaluated by the eighth-order finite difference, and spatial integrations are replaced by grid summations using the trapezoidal rule. Further details of the computations are given separately below.

A. 1D-LiH and LiH dimer models: Ground state

We consider 1D lithium hydride (LiH) and LiH dimer models. The reason for choosing these models is that they represent the simplest examples of such electronic structures with (i) deeply bound orbitals and (ii) *several* weakly bound orbitals, as shown below. These characteristics should be the key in the three-dimensional (3D) multielectron dynamics, where the existence of energetically closely-lying valence electrons is quite common, which requires to take both multichannel and multielectron effects into account. As discussed previously [62], cares have to be made for the physical soundness of 1D models. Nevertheless, we expect that the features (i) and (ii) are transferable, and 1D applications can elucidate advantages and limitations of theoretical methods, before being applied to real 3D systems.
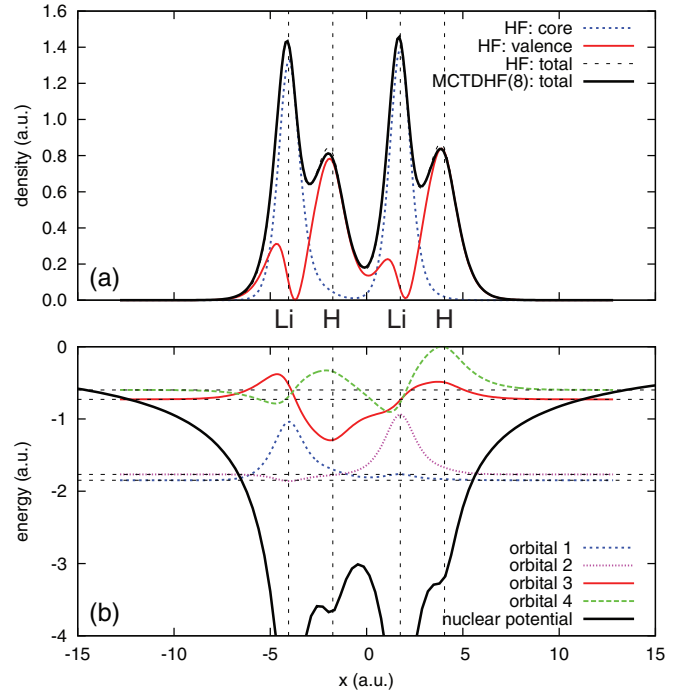

FIG. 4. (Color online) Same as Fig. 3 for the 1D-(LiH)$_2$ model. (a) The core and valence densities correspond to the contributions from orbitals 1 and 2, and from orbitals 3 and 4, respectively. (b) The orbital energies are $-1.85, -1.77, -0.73,$ and -0.60, for orbitals 1–4, respectively.

For LiH, we set the molecular parameters as $\mathbf{Z} = \{3,1\}$ and $\mathbf{X} = \{-1.15, 1.15\}$. For (LiH)$_2$, $\mathbf{Z} = \{3,1,3,1\}$ and $\mathbf{X} = \{-4.05, -1.75, +1.75, +4.05\}$. The soft Coulomb parameters $c = 0.5$ and $d = 1$ are used, since an often-made choice of $c = d = 1$ [76,77] was found to overemphasize the electron-electron repulsion. The above molecular parameters correspond to the equilibrium bond length $r = 2.3$ of Li-H and intermolecular distance $R = 3.5$ of LiH–LiH, as shown in Fig. 2, which plots several cuts of the adiabatic energy surface of (LiH)$_2$,

$$E(r,R) = \langle \Psi | H | \Psi \rangle + \sum_{a>b}^{M} \frac{Z_a Z_b}{|X_a - X_b|}. \tag{49}$$

The energy surface with parameters $c = d = 1$ predicted no stable LiH dimer in this nuclear configuration, relative to the separated LiH molecules.

To make a sensible comparison among methods with different active spaces, we consider the following wave functions for LiH:

$$\Psi_{\text{HF}} : \phi_1^2 \phi_2^2, \tag{50a}$$

$$\Psi_{\text{CASSCF}(2,n)} : \phi_1^2 (\phi_2 \phi_3 \ldots \phi_{n+1})^2, \tag{50b}$$

$$\Psi_{\text{MCTDHF}(n+1)} : (\phi_1 \phi_2 \phi_3 \ldots \phi_{n+1})^4, \tag{50c}$$

and for (LiH)$_2$:

$$\Psi_{\text{HF}} : \phi_1^2 \phi_2^2 \phi_3^2 \phi_4^2, \tag{51a}$$

$$\Psi_{\text{CASSCF}(2,n-1)} : \phi_1^2 \phi_2^2 \phi_3^2 (\phi_4 \phi_5 \ldots \phi_{n+2})^2, \tag{51b}$$

$$\Psi_{\text{CASSCF}(4,n)} : \phi_1^2 \phi_2^2 (\phi_3 \phi_4 \ldots \phi_{n+2})^4, \tag{51c}$$

$$\Psi_{\text{MCTDHF}(n+2)} : (\phi_1 \phi_2 \phi_3 \ldots \phi_{n+2})^8, \tag{51d}$$

following the notations of Eqs. (3) and (4). The CASSCF and MCTDHF wave functions are designed to consist of the same number of occupied orbitals with increasing active orbitals.

Figures 3 and 4 show the shapes of the ground-state occupied HF orbitals and the one-electron probability density for LiH and $(LiH)_2$, respectively. As seen in Fig. 3(b), the nodeless first HF orbital of LiH localizes at the Li "atom," while the second orbital is responsible for the formation of a "chemical bond," made from constructive superposition of the ground-state wave function of H and the second atomic orbital of Li, the node of the latter shifted to the bonding region. Figure 3(a) shows that the total electron density is well reproduced by the HF method compared to the MCTDHF(8) density. In Fig. 4(b), one sees that the HF orbitals of $(LiH)_2$ can be clearly separated to the deeply bound core (orbitals 1 and 2) and weakly bound valence (orbitals 3 and 4) orbitals, the former keeping the atomic-orbital characters of Li, with the latter two orbitals delocalizing across the dimer. Again, as seen in Fig. 4(a), the total density is well reproduced by HF. Finally, it is observed that the tails of the total electron density are determined by the valence electrons both in LiH and $(LiH)_2$.

Table I summarizes the ground-state calculations. As seen in the table, there are significant gaps in total energies between methods with different numbers of active electrons. However, the MCTDHF values for the other properties are reproduced rather well by the CASSCF(2,n) and CASSCF(4,n) methods for LiH and $(LiH)_2$, respectively. For instance, the difference in E_{tot} of CASSCF(4,8) and MCTDHF(10) for $(LiH)_2$ is approximately 12 mhartree, but those in IP and Δ_2 are 0.05 eV (2 mhartree) and 0.003 eV (0.2 mhartree), respectively. This says that the correlations responsible for these properties are those among the valence electrons.

The CASSCF(2,n) active spaces of Eq. (51b), with only two of four nearly degenerate electrons being correlated, are not physically sensible ones for $(LiH)_2$. Accordingly, the resulting dipole moment values are not much improved from the HF value. More seriously, the proper dissociation limit of such a wave function to the equivalent LiH molecules cannot be defined well, i.e., the formation energy Δ_2 cannot be obtained. This problem is related to the lack of the "size extensivity," [48,49,53] which fails to guarantee the equal quality of the approximation for different electronic configurations. The size-inextensive treatment covers less and less electron correlation as systems grow larger.

B. 1D LiH model: Ionization dynamics

Now we apply the TD-CASSCF method to the laser-driven electron dynamics of the 1D-LiH model. We use the three-cycle laser electric field of the following form:

$$E(t) = E_0 \sin(\omega t) \sin^2\left(\pi \frac{t}{\tau}\right), \quad 0 \leqslant t \leqslant \tau, \quad (52)$$

with $\omega = 0.06075$ (wavelength 750 nm), $\tau = 6\pi/\omega$, and three different amplitudes $E_0 = 0.0534$, 0.107, and 0.151, corresponding to peak intensities $I_0 = 1.0 \times 10^{14}$, 4.0×10^{14}, and 8.0×10^{14} W/cm^2, respectively. The Keldysh parameters are 1.30, 0.65, and 0.46, respectively, for the three intensities. In view of the ground-state electronic structure of Fig. 3 and the

TABLE I. Total energy E_{tot} in atomic unit (a.u.), dipole moment $\langle x \rangle$ in a.u., first ionization potential IP in eV, LiH formation energy Δ_1 in eV, and $(LiH)_2$ formation energy Δ_2 in eV. Results of HF, CASSCF, and MCTDHF methods with varying active spaces are compared. The ionization potential (IP) is computed as the difference of the total energies of the neutral and cationic ground states. The Δ_1 is the difference of the energy of LiH and the sum of energies of Li and H, and Δ_2 is the difference of the energy of $(LiH)_2$ and twice that of LiH. For computing Δ_1 and Δ_2 with CASSCF and MCTDHF methods, the active spaces for the fragments are the proper dissociation limit of the parent description of the complex. For HF calculations, the open-shell restricted HF method is used for doublet species. The Δ_2 of CASSCF(2,n_A) methods are not available, since their proper dissociation limits are not well defined.

	E_{tot}	$\langle x \rangle$	IP	Δ_1	Δ_2
		1D-LiH			
$N_A = 0$					
HF	−7.0664	−1.33	17.82	5.07	
$N_A = 2$					
CASSCF(2,2)	−7.0819	−1.41	18.24	5.49	
CASSCF(2,4)	−7.0847	−1.41	18.32	5.57	
CASSCF(2,8)	−7.0847	−1.41	18.32	5.57	
$N_A = 4$					
MCTDHF(3)	−7.0824	−1.41	18.15	5.51	
MCTDHF(5)	−7.0908	−1.42	18.32	5.46	
MCTDHF(9)	−7.0920	−1.42	18.35	5.48	
		1D-$(LiH)_2$			
$N_A = 0$					
HF	−14.1378	−2.31	15.57		0.135
$N_A = 2$					
CASSCF(2,3)	−14.1532	−2.36	15.99		N/A
CASSCF(2,5)	−14.1534	−2.36	16.00		N/A
CASSCF(2,7)	−14.1534	−2.36	16.00		N/A
$N_A = 4$					
CASSCF(4,4)	−14.1664	−2.45	15.80		0.071
CASSCF(4,6)	−14.1726	−2.46	15.90		0.100
CASSCF(4,8)	−14.1735	−2.46	15.92		0.114
$N_A = 8$					
MCTDHF(6)	−14.1682	−2.45	15.70		0.094
MCTDHF(8)	−14.1822	−2.48	15.85		0.110
MCTDHF(10)	−14.1859	−2.49	15.87		0.117

above laser profile, one reasonably expects that the dominant physical process involved is the tunneling ionization from the highest occupied orbital in the static HF picture. Hence, we can speculate that the two-active-electron description TD-CASSCF(2,n_A) is necessary and sufficient for the accurate description of the dynamics, as will be confirmed below.

Figure 5 shows the time evolution of the dipole moment. First we observe the large difference in the results of TDHF and other methods. For the lowest intensity of 1.0×10^{14} W/cm^2, the difference remains quantitative, largely due to the difference of the ground-state permanent dipole moment. For higher intensities, TDHF clearly underestimates the laser-driven large-amplitude electron motions. This is due to the fundamental inadequacy of the closed-shell description [Eq. (50a)] of the tunneling ionization process, which involves spatially different motions of the ionizing and nonionizing electrons. The TD-CASSCF(2,2) brings substantial improvement over the TDHF,
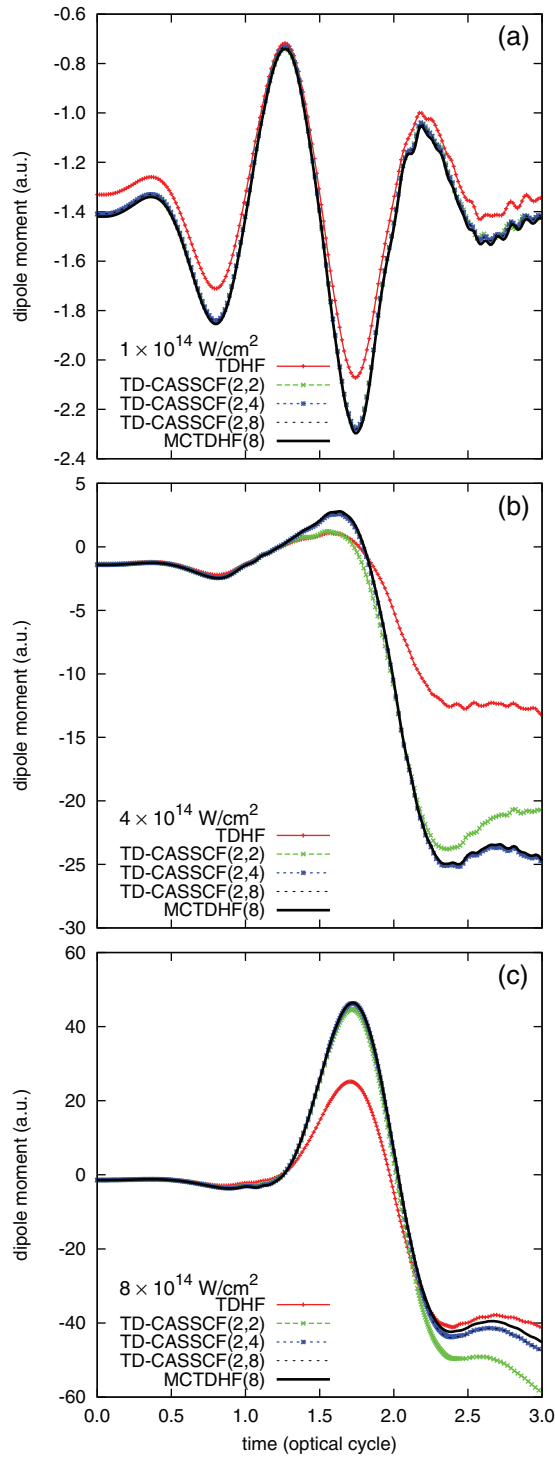
FIG. 5. (Color online) Dipole moment of the 1D-LiH model as a function of time, with peak intensities (a) 1×10^{14}, (b) 4×10^{14}, and (c) 8×10^{14} W/cm^2.

FIG. 6. (Color online) Ionization probabilities P_n of the 1D-LiH model as a function of time, with peak intensities (a) 4×10^{14} and (b) 8×10^{14} W/cm^2. TDHF (black dotted), TD-CASSCF(2,4) (colored), and MCTDHF(5) (block solid) results are compared.

giving results with much better agreement with the MCTDHF ones. The convergent description in the TD-CASSCF(2,n_A) series is obtained at $n_A = 4$. The TD-CASSCF(2,n_A) with $n_A \geqslant 4$ closely reproduce the results of MCTDHF method.

Figure 6 plots the n-electron ionization probability P_n, defined for convenience as a probability to find n electrons locate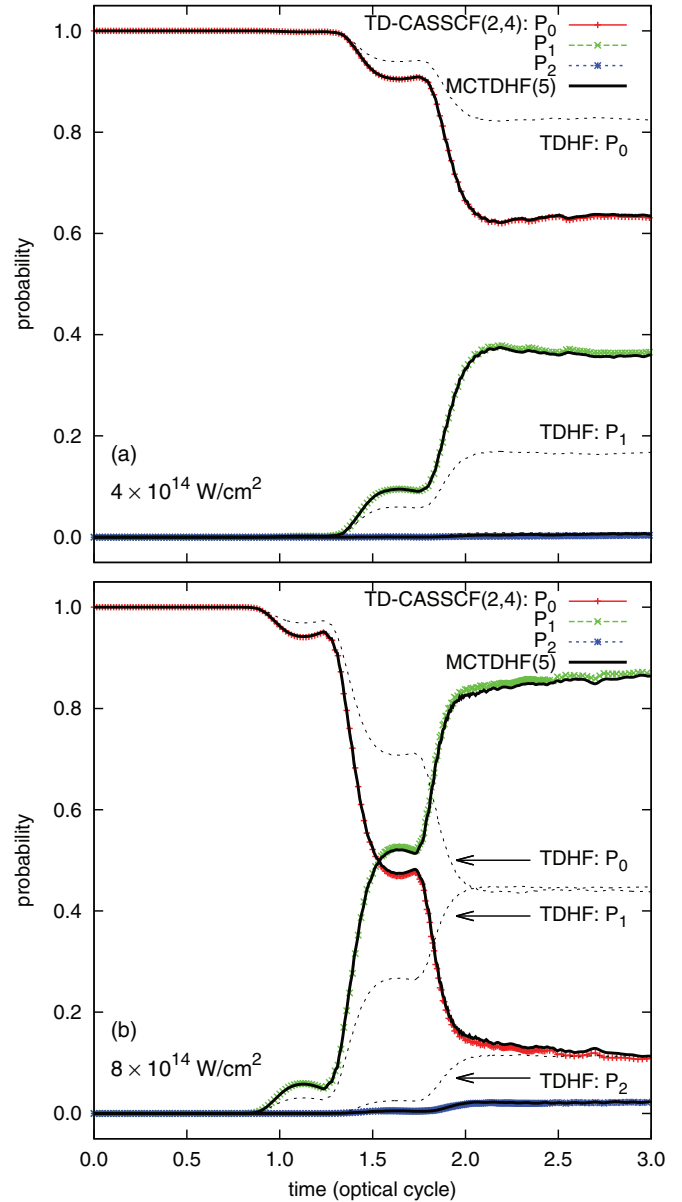d outside a given distance $R_{ion} = 20$ (see Appendix), of LiH as a function of time for the peak intensities (a) 4×10^{14} and (b) 8×10^{14} W/cm^2. No appreciable ionization is found with the lowest intensity. The probability of finding more than two ionized electrons is negligibly small for all intensities. As seen in Fig. 6, TD-CASSCF(2,4) gives virtually the same results as MCTDHF(5). The TDHF method, on the other hand, underestimates single ionization P_1 and, at the higher intensity, unphysically overestimates double ionization P_2. This is the consequence of forcing two valence electrons to travel with a single spatial orbital.

These results demonstrate that the TD-CASSCF(2,2) constitutes the simplest method to describe the present dynamics in a physically correct way. Its total wave function can be

written as

$$\Psi = \hat{A}[\phi_1\bar{\phi}_1\{C_1\phi_2\bar{\phi}_2 + C_2\phi_3\bar{\phi}_3\}] \tag{53}$$

in the natural orbital representation [78,79], where ϕ_i ($\bar{\phi}_i$) is an orbital occupied by up (down) spin electrons. The two-configuration CI part of Eq. (53) can be transformed back to the nonorthogonal expression [Eq. (1a)],

$$\Psi \propto \hat{A}\left[\phi_1\bar{\phi}_1\left\{(\psi_1\psi_2 + \psi_2\psi_1)\frac{1}{\sqrt{2}}(\alpha\beta - \beta\alpha)\right\}\right], \tag{54}$$

giving a clearer picture of different spatial motions of the two valence electrons, with [48]

$$|\langle\psi_1|\psi_2\rangle| = \frac{|C_1| - |C_2|}{|C_1| + |C_2|}. \tag{55}$$

The flexibility inherent in Eqs. (53) or (54) enables a seamless transition from the closed-shell-dominant ground state ($|C_1| \gg |C_2| \Longleftrightarrow \langle\psi_1|\psi_2\rangle \approx 1$) to the single ionization limit ($|C_1| \approx |C_2| \Longleftrightarrow \langle\psi_1|\psi_2\rangle \approx 0$). The ionization dynamics, therefore, is characterized by the *strong* or *static* correlation [48,49,52,53] in the sense that it involves drastic changes of the configuration weights (the magnitudes of CI coefficients) with more than one determinant contributing significantly. The failure of single-determinant TDHF to describe the ionization process is attributed to the lack of this type of correlation.

For a quantitatively accurate description of the dynamics, the above minimum CI wave function has to be improved by incorporating more-than-two active orbitals, as seen in the convergence of the dipole moments in Fig. 5 with respect to the number of active orbitals. The agreement of TD-CASSCF($2,n_A$) and MCTDHF results indicates that the core electron correlation is not relevant, at the first approximation, for the ionization dynamics induced by the present laser field. The TD-CASSCF allows the compact representation of such physical situations.

C. 1D-LiH dimer model: Ionization dynamics

In this section, we proceed to the multielectron dynamics of the 1D-(LiH)$_2$ model. We assess TDHF, TD-CASSCF(2,7), TD-CASSCF(4,8), and MCTDHF(10) methods. These active spaces are shown in Eq. (51) with $n = 8$. The latter two are twice the size of those in TD-CASSCF(2,4) and MCTDHF(5) for LiH, respectively, which have been confirmed to provide the convergent description in Sec. III B.

Figure 7 shows the temporal evolution of the dipole moment simulated with various methods. One clearly sees that TDHF and TD-CASSCF(2,7) results show large deviations from the MCTDHF(10) results, while TD-CASSCF(4,8) reproduces the results of MCTDHF(10) fairly well. This indicates that all the four valence electrons sketched in Fig. 4 actively participate in the field-induced ionization dynamics (this does not necessarily mean that the four electrons are ionized), while tightly bound core electrons remain nonionized. For the ionizing electrons, the closed-shell description is inadequate, as discussed in Sec. III B.

In Figs. 8 and 9, we compare the temporal evolution of the ionization probability P_n with $R_{ion} = 20$ of (LiH)$_2$ computed by approximate methods and MCTDHF(10). As can be seen from Fig. 8, both TDHF and TD-CASSCF(2,7) methods

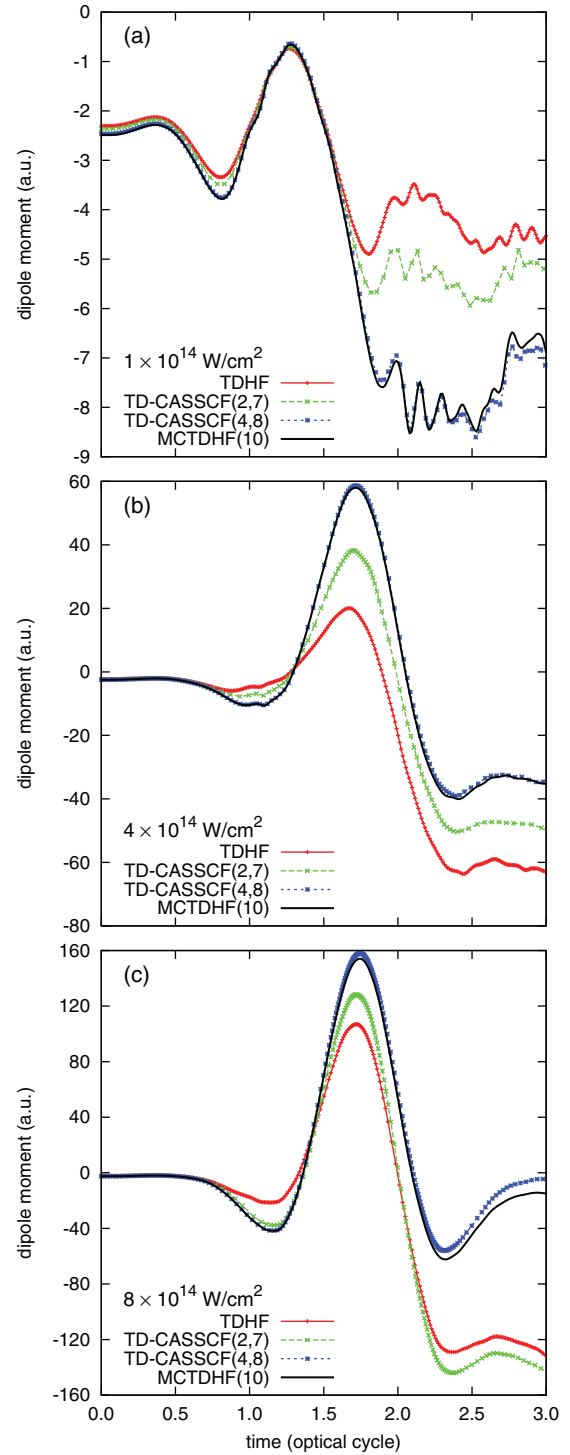FIG. 7. (Color online) Dipole moment of the 1D-(LiH)$_2$ model as a function of time, with peak intensities (a) 1×10^{14}, (b) 4×10^{14}, and (c) 8×10^{14} W/cm^2. Results of TDHF, TD-CASSCF(2,7), TD-CASSCF(4,8), and MCTDHF(10) methods are compared.

tend to underestimate single ionization for all the examined intensities. The probability of finding more than two ionized electrons is found to be erroneous in an inconsistent way, and is thus not shown. In a striking contrast, TD-CASSCF(4,8) well reproduces the ionization probability P_n of MCTDHF(10) [Figs. 9(a)–9(c)]. Slight deviation is seen only at the later stage
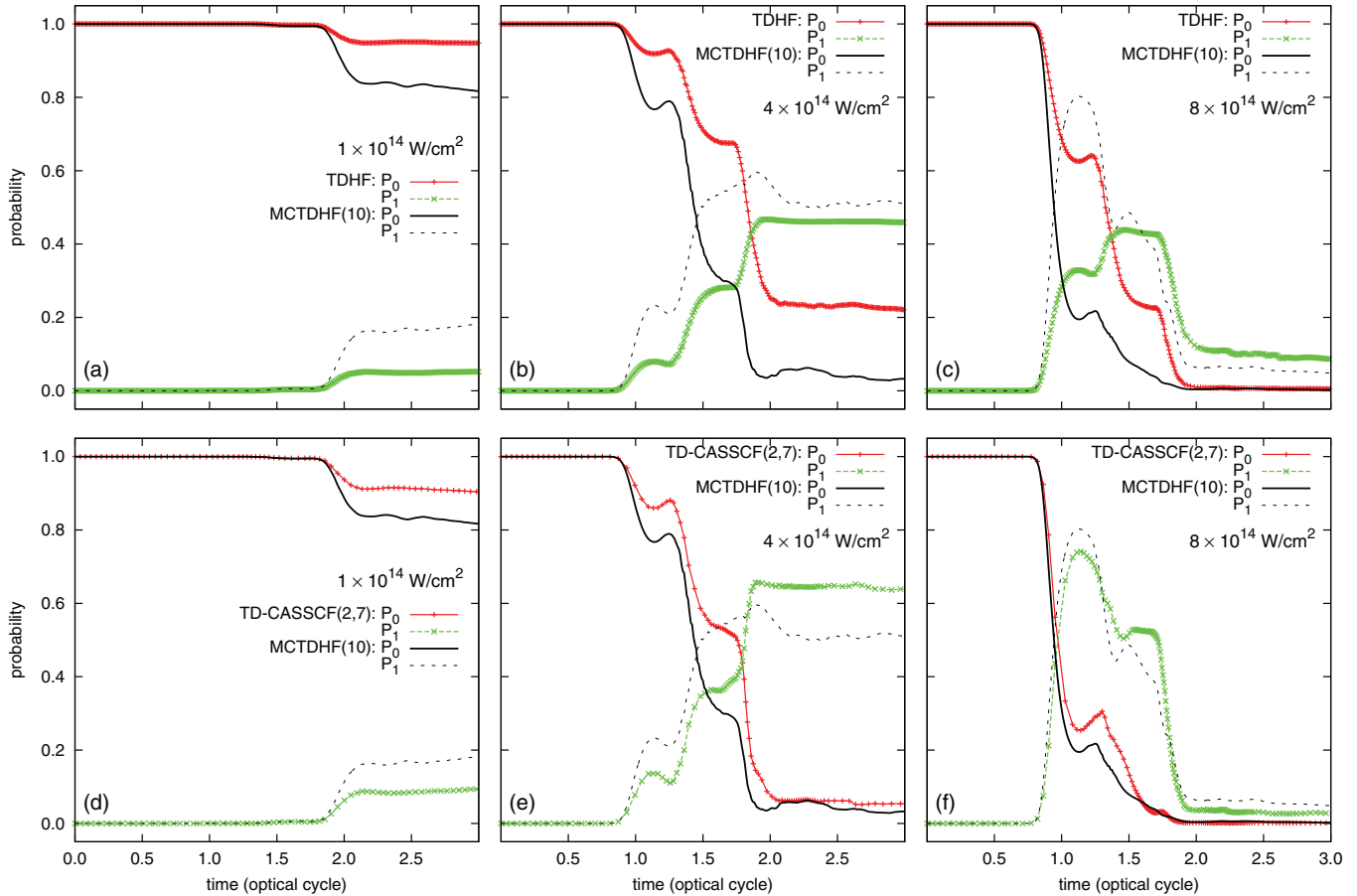
FIG. 8. (Color online) Ionization probabilities P_0 and P_1 of the 1D-$(LiH)_2$ model as a function of time, with peak intensities 1×10^{14} (left), 4×10^{14} (center), and 8×10^{14} W/cm^2 (right). Results of TDHF (top) and TD-CASSCF(2,7) (bottom) are compared with those of MCTDHF (black solid and dotted).

of the pulse for the higher intensities. The inclusion of more active orbitals would further improve the agreement.

So far, all the core orbitals have been treated as dynamical core orbitals. In Figs. 9(d)–9(f), the ionization probabilities computed with TD-CASSCF(4,8), with all the core orbitals treated as frozen, denoted TD-CASSCF(4,8)-FC, are shown. It reproduces the results of MCTDHF(10) almost as nicely as TD-CASSCF(4,8) with dynamical-core orbitals, which indicates that the core polarization plays minor roles in the present dynamics.

It is worth noting that even at the lowest intensity 1.0×10^{14} W/cm^2 dominated by single ionization, the TD-CASSCF(2,7) fails to give an accurate value of P_1 but underestimates it roughly by half [Fig. 8(d)]. This implies the importance of the multichannel ionization, which can be described correctly only when all the relevant orbitals are included in the active space. On the other hand, at higher intensities, the total wave function consists of the widespread superposition of the ground, excited, and continuum states. For a balanced description, each of these components has to be treated with an equal quality, which requires a size-extensive theory. The MCTDHF, as the exact theory within a given number of time-dependent bases, fulfills the size-extensivity condition. The TD-CASSCF with a proper active space preserves this important property of the MCTDHF. It is demon-

strated by the accurate multiple ionization probabilities of the TD-CASSCF(4,8) method, up to P_4 for the highest intensity in Fig. 9(c). The importance of selecting an appropriate active space is illustrated by the fact that the TD-CASSCF(4,n_A) is required for $(LiH)_2$, while the TD-CASSCF(2,n_A) is adequate for LiH.

D. Analyses of computational cost

Table II summarizes computational times for simulations of the 1D-$(LiH)_2$ model with a peak intensity 4×10^{14} W/cm^2. To highlight the different computational bottlenecks discussed in Sec. II D, several box sizes (N_b = 1000, 2000, and 3000) are considered. The CPU times in Table II(a), II(b), and II(c) are recorded on a single Xeon processor of clock frequency 3.33 GHz for propagating 1000 time steps during $2T \leqslant t \leqslant 2.1T$ with the fixed step-size RK4 algorithm, where $T = 2\pi/\omega$. Entry (d) compares wall clock times spent for completing the simulation up to four optical cycles ($0 \leqslant t \leqslant 4T$), with the VRK5 algorithm, measured for multi-threaded computations using 12 processors.

First, as seen in Table II(a), CPU times for procedure (A) grow rapidly with increasing CI dimension, reproducing the theoretical linear dependence on N_{det}. These timings marginally depend on N_b. Next, CPU times for procedure

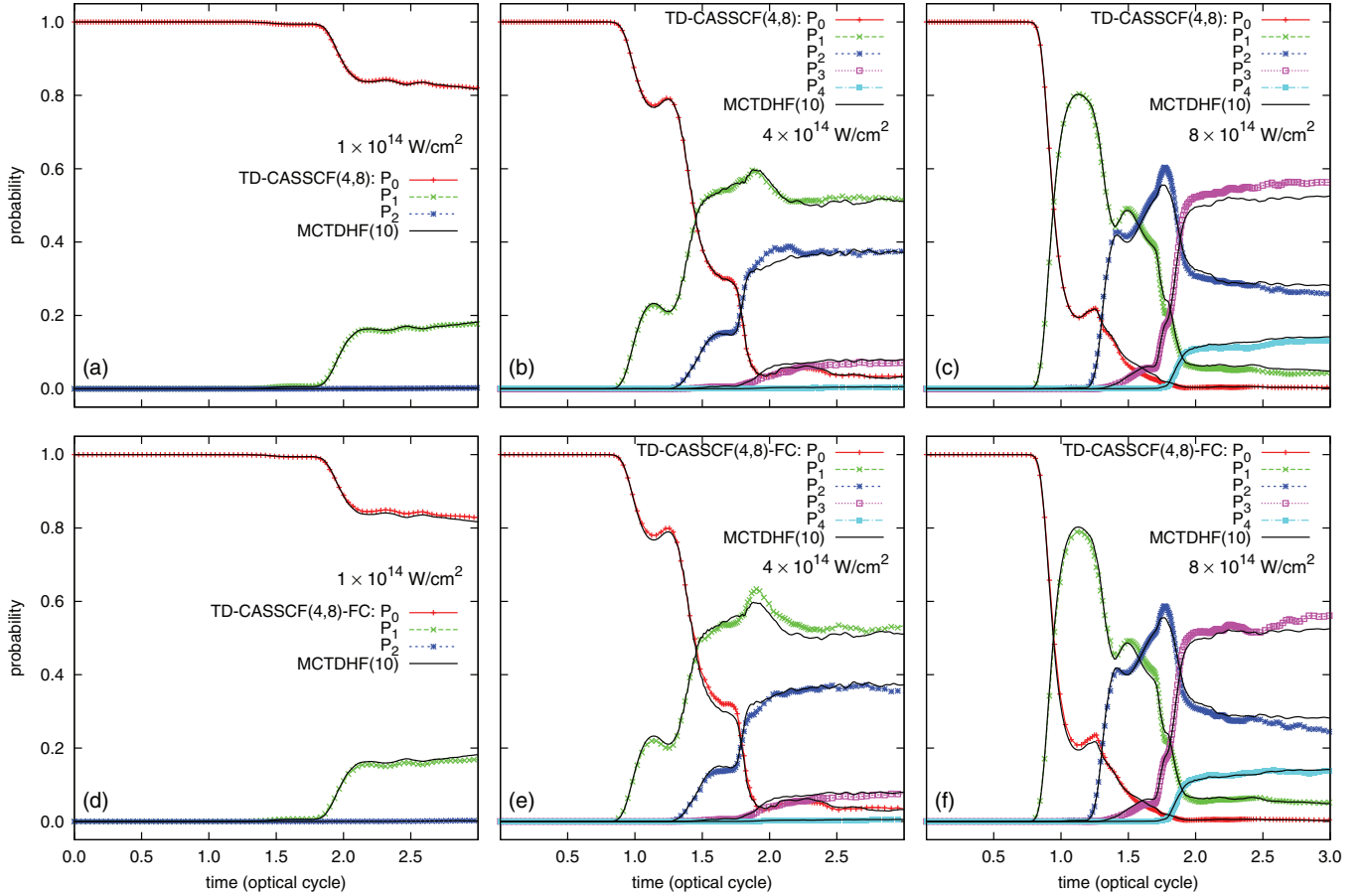FIG. 9. (Color online) Ionization probabilities P_n with $n \leqslant 4$ of the 1D-(LiH)$_2$ model as a function of time, with peak intensities 1×10^{14} (left), 4×10^{14} (center), and 8×10^{14} W/cm^2 (right). Results of TD-CASSCF(4,8) (top) and TD-CASSCF(4,8)-FC (bottom) are compared with those of MCTDHF (black solid).

(B) in Table II(b) scale as $O(N_b^d)$ with $d = 1.95, 1.67, 1.66$, and 1.47 for TDHF, TD-CASSCF(2,7), TD-CASSCF(4,8), and MCTDHF(10) methods, respectively. This is the consequence of competing $O(n^2 N_b^2)$ and $O(n_A^4 N_b)$ contributions as discussed in Sec. II D, with growing importance of the latter for larger active spaces. The TD-CASSCF(4,8)-FC demands less CPU time than the TD-CASSCF(4,8), due to the strict locality of frozen-core orbitals, limiting the range of exchange operators $\hat{K}_i |\phi_t\rangle$ around the core region.

Net CPU times are listed in Table II(c). In TDHF and TD-CASSCF calculations with core subspaces, the grid-intensive procedure (B) is definitely rate limiting. In contrast, MCTDHF calculations involve severe bottlenecks both in procedures (A) and (B). The N_{det}-dependent works dominate 85%, 67%, and 55% of the net CPU times, with $N_b = 1000, 2000$, and 3000, respectively. The cost reduction achieved by the TD-CASSCF method largely depends on the relative importance of procedures (A) and (B). Ratios of net CPU times for TD-CASSCF(4,8) and MCTDHF(10) calculations are 0.12, 0.29, and 0.45 with $N_b = 1000, 2000, 3000$, respectively. Similar trends are observed for wall clock times with the VRK5 algorithm, as seen in Table II(d). The stability of EOMs is found to be similar for the tested methods, requiring about 70 000 evaluations of EOMs. The cost gain by the TD-CASSCF method relative to the MCTDHF method will be more drastic if

$N_A \ll N$. However, an efficient implementation of the mean-field potential [Eq. (32)] is essential to achieve further speedup for large N_b, especially in three-dimensional applications.

IV. CONCLUSIONS

We have developed a new *ab initio* time-dependent many-electron method called TD-CASSCF. It applies the concept of CASSCF, which has been developed for the electronic structure calculation in quantum chemistry, to the multielectron dynamics in intense laser fields, introducing frozen-core, dynamical-core, and active orbital subspaces. The classification into the subspaces can be done by flexibly conforming to simulated physical situations and desired accuracy, and both TDHF and MCTDHF methods are included as special cases. This feature enables compact yet accurate representation of ionization dynamics in many-electron systems, and bridges the huge gap between TDHF and MCTDHF methods.

We have applied the TD-CASSCF method to the ionization dynamics of 1D-LiH and 1D-(LiH)$_2$ to assess its capability of describing multichannel and multielectron ionization. It has been confirmed that the present method closely reproduces rigorous MCTDHF results if the active orbital space is properly chosen to include appreciably ionizing electrons. We have also confirmed that the TD-CASSCF provides substantial

TABLE II. Computational times for simulations of the 1D-$(LiH)_2$ model. First row: Numbers of determinant N_{det} within the symmetry of zero spin projection. Entries (a), (b), and (c): CPU times in minutes for (A), (B), and overall procedures defined in Sec. II D, respectively. Entry (d): Wall clock times in minutes spent to complete the propagation of four optical cycles. Different simulation boxes are employed: $L = 200$ ($N_b = 1000$), $L = 400$ ($N_b = 2000$), and $L = 600$ ($N_b = 3000$). See text for more details.

	TDHF	TD-CASSCF			MCTDHF
Active space	(0,0)	(2,7)	(4,8)	(4,8)-FC	(8,10)
N_{det}	1	49	784	784	44 100
(a) RK4/1000 steps, CPU-A					
$N_b = 1000$	0.0	0.1	1.2	1.2	212.4
$N_b = 2000$	0.0	0.2	1.3	1.3	215.1
$N_b = 3000$	0.0	0.3	1.4	1.4	215.3
(b) RK4/1000 steps, CPU-B					
$N_b = 1000$	4.3	26.8	28.4	22.0	35.7
$N_b = 2000$	16.3	87.6	90.9	73.8	103.5
$N_b = 3000$	36.8	168.0	175.4	132.9	177.2
(c) RK4/1000 steps, CPU net					
$N_b = 1000$	4.4	27.0	29.8	23.4	248.9
$N_b = 2000$	16.4	88.1	92.5	75.4	319.4
$N_b = 3000$	36.9	168.7	177.3	134.7	393.5
(d) VRK5/4 cycles, Wall					
$N_b = 1000$	8.2	43.7	51.3	39.1	451.5
$N_b = 2000$	31.0	174.8	192.6	141.4	628.8
$N_b = 3000$	65.2	378.5	394.0	282.9	823.1

computational cost reduction in the CI-length-dependent procedures, which scale by far the steepest with the system size in the MCTDHF method. Therefore the TD-CASSCF method is most advantageous for problems in which only a few weakly bound electrons out of a large number of total electrons ionize.

While it is sometimes stated that the MCTDHF method is a time-dependent version of the CASSCF method [60,61], this statement is even more suitable for the TD-CASSCF method introduced in the present study. With reduced computational cost, the TD-CASSCF method with a properly chosen active space preserves most of the theoretically important properties of the MCTDHF: (i) flexibility to account for the strong correlation involved in the ionization dynamics, (ii) size extensivity, essential for a balanced description of different electronic configurations, (iii) gauge invariance by virtue of the time-dependent variational optimization of orbitals, and (iv) invariance against orbital transformation within an orbital subspace, allowing e.g., the faithful natural orbital analyses of the time-dependent wave function [80].

It should be noted that the computational cost of the TD-CASSCF method still scales factorially with the number of active (not total) electrons; thus its applications are limited to, say, 16 half-filled active orbitals in view of the present state of the art in quantum chemistry. An example requiring such a large active space is the ionization from densely lying multiple valence orbitals in weakly interacting molecular clusters. To approach to such a problem, more restricted (instead of complete) constructions of the active space will

be necessary [73]. Moreover, a breakthrough is needed to represent one-particle wave functions in the general molecular potential without particular symmetries. In spite of these challenges, we foresee that the TD-CASSCF method will find fruitful applications in multielectron dynamics of, e.g., rare gas atoms heavier than helium, or molecules composed of atoms in the first few rows of the periodic table, exposed to visible-to-midinfrared high-intensity pulses, which are inaccessible with the all-electron-active MCTDHF method.

APPENDIX: CALCULATION OF IONIZATION PROBABILITIES

To conveniently evaluate the multiple ionization yields in many electron systems, we introduce a domain-based ionization probability P_n, defined as a probability to find n electrons in the outer region $|r| > R_{ion}$ and the remaining $N - n$ electrons in the inner region $|r| < R_{ion}$, with a given distance R_{ion} from the origin,

$$P_n \equiv \binom{N}{n} \int_> dx_1 \cdots \int_> dx_n \int_< dx_{n+1} \cdots \int_< dx_N$$
$$\times \Psi^*(x_1, \ldots, x_N) * \Psi(x_1, \ldots, x_N), \quad \text{(A1)}$$

where $\int_<$ and $\int_>$ symbolize integrations over a spatial-spin variable $x = \{r, \xi\}$ with the spatial part restricted to the domains $|r| < R_{ion}$ and $|r| > R_{ion}$, respectively.

It is convenient to introduce an auxiliary quantity T_n obtained by replacing the outer-region integrals in Eq. (A1) with the full-region ones ($\int_> \rightarrow \int$). It relates to P_n as

$$P_n = \sum_{k=0}^{n} \binom{N-n+k}{k} (-1)^k T_{n-k}. \quad \text{(A2)}$$

By adopting the CI expansion of Eq. (8), and making use of the orthonormality of spin orbitals in the full-space integration, we have

$$T_n = \sum_{IJ}^{\Pi} C_I^* C_J D_{IJ}^{(n)}, \quad \text{(A3)}$$

where

$$D_{IJ}^{(0)} = \sum_{ij}^{N} \det(S_{IJ}^<),$$

$$D_{IJ}^{(1)} = \sum_{ij}^{N} \epsilon_{ij}^{IJ} \det(S_{IJ}^<[i:j]), \quad \text{(A4)}$$

$$D_{IJ}^{(2)} = \sum_{i>j}^{N} \sum_{k>l}^{N} \epsilon_{ik}^{IJ} \epsilon_{jl}^{IJ} \det(S_{IJ}^<[ij:kl]),$$

etc., and $S_{IJ}^<$ is an $N \times N$ matrix with its $\{ij\}$ element being the inner-region overlap integral,

$$(S_{IJ}^<)_{ij} = \int_< dx \phi_{p(i,I)}^*(x)\phi_{q(j,J)}(x) \equiv \langle \phi_p | \phi_q \rangle_<, \quad \text{(A5)}$$

where $\phi_{p(i,I)}$ is the ith (in a predefined order) spin orbital in the determinant I. $S_{IJ}^<[ij\cdots:kl\cdots]$ is the submatrix of $S_{IJ}^<$ obtained after removing rows $i,j,\ldots$ and columns $k,l,\ldots$ from the latter, and

$$\epsilon_{ij}^{IJ} = \delta_{q(j,J)}^{p(i,I)}(-1)^{i+j}. \quad \text{(A6)}$$

The matrix $S_{IJ}^<$ and its submatrices are block diagonal due to the spin orthonormality, so that, e.g., $\det(S_{IJ}^<) = \det(S_{I^\alpha J^\alpha})\det(S_{I^\beta J^\beta})$, where I^σ is the σ-spin part of the determinant I.

The procedure given above remains a manageable task in the present applications, up to eight (all) electron ionization probabilities in the 1D-(LiH)$_2$ model. While this scheme becomes impractical for systems with more electrons, it may still be useful for problems where only a few electrons are ejected appreciably, since the dimension of Eqs. (A4) can be reduced to the number of the ionizing electrons.

This approach allows the evaluation of multiple ionization yields by using the information of the inner region orbitals $\langle \phi_p | \phi_q \rangle_<$ and the formal orthonormality relation $\delta_q^p = \langle \phi_p | \phi_q \rangle_< + \langle \phi_p | \phi_q \rangle_>$. It works with a reasonable size of the simulation box L, provided that $R_{\text{ion}} \ll L$, and a good absorber is implemented to prevent the reflection of the wave function. In fact, we performed calculations for the 1D-(LiH)$_2$ model in Sec. III using smaller boxes with $L = 200$ and 400 a.u., where a sizable portion of the norm is lost at the boundary, and confirmed that the obtained ionization yields are virtually the same with those of Figs. 8 and 9. Such small-scale calculations could serve as preliminary validations for the choice of the active space before stepping into large-scale computations.

[1] D. Strickland and G. Mourou, Opt. Commun. **56**, 219 (1985).

[2] S.-W. Bahk, P. Rousseau, T. A. Planchon, V. Chvykov, G. Kalintchenko, A. Maksimchuk, G. A. Mourou, and V. Yanovsky, Opt. Lett. **29**, 2837 (2004).

[3] V. Yanovsky, V. Chvykov, G. Kalinchenko, P. Rousseau, T. Planchon, T. Matsuoka, A. Maksimchuk, J. Nees, G. Cheriaux, G. Mourou, and K. Krushelnick, Opt. Express **16**, 2109 (2008).

[4] T. J. Yu, S. K. Lee, J. H. Sung, J. W. Yoon, T. M. Jeong, and J. Lee, Opt. Express **20**, 10807 (2012).

[5] M. Protopapas, C. H. Keitel, and P. L. Knight, Rep. Prog. Phys. **60**, 389 (1997).

[6] T. Brabec and F. Krausz, Rev. Mod. Phys. **72**, 545 (2000).

[7] J. Seres, E. Seres, A. J. Verhoef, G. Tempea, C. Streli, P. Wobrauschek, V. Yakovlev, A. Scrinzi, C. Spielmann, and F. Krausz, Nature (London) **433**, 596 (2005).

[8] Z. Chang, *Fundamentals of Attosecond Optics* (CRC Press, Boca Raton, FL, 2011).

[9] J. Itatani, J. Levesque, D. Zeidler, H. Niikura, H. Pèpin, J. C. Kieffer, P. B. Corkum, and D. M. Villeneuve, Nature (London) **432**, 867 (2004).

[10] S. Haessler, J. Caillat, W. Boutu, C. Giovanetti-Teixeira, T. Ruchon, T. Auguste, Z. Diveki, P. Breger, A. Maquet, B. Carré, R. Taïeb, and P. Salières, Nat. Phys. **6**, 200 (2010).

[11] P. Salières, A. Maquet, S. Haessler, J. Caillat, and R. Taïeb, Rep. Prog. Phys. **75**, 062401 (2012).

[12] P. Agostini and L. F. DiMauro, Rep. Prog. Phys. **67**, 813 (2004).

[13] F. Krausz and M. Ivanov, Rev. Mod. Phys. **81**, 163 (2009).

[14] L. Gallmann, C. Cirelli, and U. Keller, Annu. Rev. Phys. Chem. **63**, 447 (2013).

[15] T. Sekikawa, A. Kosuge, T. Kanai, and S. Watanabe, Nature (London) **432**, 605 (2004).

[16] Y. Nabekawa, H. Hasegawa, E. J. Takahashi, and K. Midorikawa, Phys. Rev. Lett. **94**, 043001 (2005).

[17] M. S. Pindzola and F. Robicheaux, Phys. Rev. A **57**, 318 (1998).

[18] M. S. Pindzola and F. Robicheaux, J. Phys. B **31**, L823 (1998).

[19] J. Colgan, M. S. Pindzola, and F. Robicheaux, J. Phys. B **34**, L457 (2001).

[20] J. S. Parker, L. R. Moore, K. J. Meharg, D. Dundas, and K. T. Taylor, J. Phys. B **34**, L69 (2001).

[21] S. Laulan and H. Bachau, Phys. Rev. A **68**, 013409 (2003).

[22] B. Piraux, J. Bauer, S. Laulan, and H. Bachau, Eur. Phys. J. D **26**, 7 (2003).

[23] S. Laulan and H. Bachau, Phys. Rev. A **69**, 033408 (2004).

[24] K. L. Ishikawa and K. Midorikawa, Phys. Rev. A **72**, 013407 (2005).

[25] J. Feist, S. Nagele, R. Pazourek, E. Persson, B. I. Schneider, L. A. Collins, and J. Burgdörfer, Phys. Rev. Lett. **103**, 063002 (2009).

[26] R. Pazourek, J. Feist, S. Nagele, E. Persson, B. I. Schneider, L. A. Collins, and J. Burgdörfer, Phys. Rev. A **83**, 053418 (2011).

[27] K. L. Ishikawa and K. Ueda, Phys. Rev. Lett. **108**, 033003 (2012).

[28] S. Sukiasyan, K. L. Ishikawa, and M. Ivanov, Phys. Rev. A **86**, 033423 (2012).

[29] K. L. Ishikawa and K. Ueda, Appl. Sci. **3**, 189 (2013).

[30] W. Vanroose, D. A. Horner, F. Martín, T. N. Rescigno, and C. W. McCurdy, Phys. Rev. A **74**, 052702 (2006).

[31] D. A. Horner, S. Miyabe, T. N. Rescigno, C. W. McCurdy, F. Morales, and F. Martín, Phys. Rev. Lett. **101**, 183002 (2008).

[32] T.-G. Lee, M. S. Pindzola, and F. Robicheaux, J. Phys. B **43**, 165601 (2010).

[33] A. Gordon, F. X. Kärtner, N. Rohringer, and R. Santra, Phys. Rev. Lett. **96**, 223902 (2006).

[34] N. Rohringer and R. Santra, Phys. Rev. A **79**, 053402 (2009).

[35] O. Smirnova, S. Patchkovskii, Y. Mairesse, N. Dudovich, and M. Y. Ivanov, Proc. Natl. Acad. Sci. USA **106**, 16556 (2009).

[36] H. Akagi, T. Otobe, A. Staudte, A. Shiner, F. Turner, R. Dörner, D. M. Villeneuve, and P. B. Corkum, Science **325**, 1364 (2009).

[37] A. E. Boguslavskiy, J. Mikosch, A. Gijsbertsen, M. Spanner, S. Patchkovskii, N. Gador, M. J. J. Vrakking, and A. Stolow, Science **335**, 1336 (2012).

[38] J. Caillat, J. Zanghellini, M. Kitzler, O. Koch, W. Kreuzer, and A. Scrinzi, Phys. Rev. A **71**, 012712 (2005).

[39] N. Rohringer, A. Gordon, and R. Santra, Phys. Rev. A **74**, 043420 (2006).

[40] L. Greenman, P. J. Ho, S. Pabst, E. Kamarchik, D. A. Mazziotti, and R. Santra, Phys. Rev. A **82**, 023406 (2010).

[41] E. K. U. Gross, J. F. Dobson, and M. Petersilka, Top. Curr. Chem. **181**, 81 (1996).

[42] T. Otobe, K. Yabana, and J.-I. Iwata, Phys. Rev. A **69**, 053404 (2004).

[43] D. A. Telnov and S.-I. Chu, Phys. Rev. A **80**, 043412 (2009).

[44] S. Kvaal, J. Chem. Phys. **136**, 194109 (2012).

[45] C. Huber and T. Klamroth, J. Chem. Phys. **134**, 054113 (2011).

[46] D. Hochstuhl and M. Bonitz, Phys. Rev. A **86**, 053424 (2012).

[47] J. Olsen, B. O. Roos, P. Jørgensen, and H. J. A. Jensen, J. Chem. Phys. **89**, 2185 (1988).

[48] A. Szabo and N. S. Ostlund, *Modern Quantum Chemistry* (Dover, Mineola, 1996).

[49] T. Helgaker, P. Jørgensen, and J. Olsen, *Molecular Electronic-Structure Theory* (Wiley, New York, 2002).

[50] K. Ruedenberg, M. W. Schmidt, M. M. Gilbert, and S. T. Elbert, Chem. Phys. **71**, 41 (1982).

[51] B. O. Roos, P. R. Taylor, and P. E. M. Siegbahn, Chem. Phys. **48**, 157 (1980).

[52] B. O. Roos, Adv. Chem. Phys. **69**, 399 (1987).

[53] M. W. Schmidt and M. S. Gordon, Annu. Rev. Phys. Chem. **49**, 233 (1998).

[54] M. S. Pindzola, D. C. Griffin, and C. Bottcher, Phys. Rev. Lett. **66**, 2305 (1991).

[55] M. S. Pindzola, F. Robicheaux, and P. Gavras, Phys. Rev. A **55**, 1307 (1997).

[56] A. J. Tolley, J. Phys. B **32**, 3449 (1999).

[57] N. E. Dahlen and R. van Leeuwen, Phys. Rev. A **64**, 023405 (2001).

[58] N. A. Nguyen and A. D. Bandrauk, Phys. Rev. A **73**, 032708 (2006).

[59] T. Kato and H. Kono, Chem. Phys. Lett. **392**, 533 (2004).

[60] M. Nest, T. Klamroth, and P. Saalfrank, J. Chem. Phys. **122**, 124102 (2005).

[61] M. Nest and T. Klamroth, Phys. Rev. A **72**, 012710 (2005).

[62] G. Jordan, J. Caillat, C. Ede, and A. Scrinzi, J. Phys. B **39**, S341 (2006).

[63] T. Kato and H. Kono, J. Chem. Phys. **128**, 184102 (2008).

[64] O. E. Alon, A. I. Streltsov, and L. S. Cederbaum, J. Chem. Phys. **127**, 154103 (2007).

[65] D. Hochstuhl and M. Bonitz, J. Chem. Phys. **134**, 084106 (2011).

[66] R. P. Miranda, A. J. Fisher, L. Stella, and A. P. Horsfield, J. Chem. Phys. **134**, 244101 (2011).

[67] M. H. Beck, A. Jäckle, G. A. Worth, and H.-D. Meyer, Phys. Rep. **324**, 1 (2000).

[68] X. Li, S. M. Smith, A. N. Markevitch, D. A. Romanov, R. J. Levis, and H. B. Schlegel, Phys. Chem. Chem. Phys. **7**, 233 (2005).

[69] J. Frenkel, *Wave Mechanics–Advanced General Theory* (Clarendon Press, Oxford, 1934).

[70] P.-O. Löwdin and P. K. Mukherjee, Chem. Phys. Lett. **14**, 1 (1972).

[71] R. Moccia, Int. J. Quantum Chem. **7**, 779 (1973).

[72] P. J. Knowles and N. C. Handy, Comput. Phys. Commun. **54**, 75 (1988).

[73] H. Miyagi and L. B. Madsen, Phys. Rev. A **87**, 062511 (2013).

[74] B. Levy and G. Berthier, Int. J. Quantum Chem. **2**, 307 (1968).

[75] B. Levy and G. Berthier, Int. J. Quantum Chem. **3**, 247 (1969).

[76] K. Balzer, S. Bauch, and M. Bonitz, Phys. Rev. A **81**, 022510 (2010).

[77] K. Balzer, S. Bauch, and M. Bonitz, Phys. Rev. A **82**, 033427 (2010).

[78] W. Kutzelnigg, Theor. Chim. Acta **1**, 327 (1963).

[79] W. Kutzelnigg, J. Chem. Phys. **40**, 3640 (1964).

[80] T. Kato and H. Kono, Chem. Phys. **366**, 46 (2009).